Modelling of Ductile Rupture of Bi-Material Components Using Local Approach

Y. Madi[1], J. Besson[1]

[1] Ecoles des Mines de Paris, Centre des Matériaux, UMR CBRS 7633 BP 87, 91003 Evry Cedex, France. E-mail: madi@mat.ensmp.fr or besson@mat.ensmp.fr

ABSTRACT. *The safety assessment of welded structures still remains an important industrial problem. In this study, a simple diffusion bonded bi-material junction has been made in order to analyse the Mismatch effect. It consists of an assembly of ferritic and austenitic steels which are representative of nuclear pressure vessel. Tests were performed on various specimens including: smooth and notched tensile bars, Charpy specimens and single-edge notch bend specimens. Homogeneous and bimaterial structures were tested. Smooth and notch tensile bars tests were used to adjust the parameters of local approach based on the Gurson model according to the "local approach of fracture" procedure. On deeply notched specimens, the effect of the distance between the notch root and the interface on fracture initiation and crack propagation direction was studied. Tests were modeled using elasto–plastic finite element simulations. The correct test/computation agreement shows that the adjusted parameters on the homogeneous specimens can be transferred to heterogeneous structures. In particular, simulation well reproduces the experimental crack path bifurcation.*

INTRODUCTION

The structural safety assessment of welded structures (particularly bi-material components) remains an important industrial problem. The interaction between the welded parts, the weld metal and the heat affected zones makes the structural integrity analysis difficult. Geometrical details of the weld may make the problem even more complex.

In this study, a simple diffusion bonded bimaterial joint was produced in order to analyze the strength mismatch effect on damage process at the interface region. It consists of an assembly of ferritic and austenitic steels which are representative of bi-material components used in nuclear pressure vessels. In that case, the joint is welded so that the situation to be analysed is more complex. The bonded joint studied in this work is therefore a simplified representation of the actual structure.

The microstructures of each material are first presented. The interface region was analyzed using microprobe analysis. Then the mechanical and fracture behaviours are studied using smooth and notched tensile bars (NT), Charpy V-notch specimens and

single edge eotch bend (SENB) specimens. Crack paths and failure mode under static loading are then examined.

Due to the complex nature of welds, the local approach to fracture, [1], is well suited to analyse the fracture behavior of such constituants. This approach is able to deal with situations where no preexisting crack is present and to predict both the location of crack initiation and crack path. It is based on the analysis of local stress and strain fields at the vicinity of defects or cracks; the analysis is then coupled with damage and failure criteria which allow the determination of macroscopic fracture parameters (e.g. load to failure) as well as fracture path. In this work, material damage and failure are described using the Gurson model, [2]. Parameters of the damage model for both constituents are determined on homogeneous samples and used to simulate the fracture of heterogeneous structures using the Finite Element (FE) method.

MATERIALS AND TESTING

Materials
The study was performed on a bi-material junction consisting of a ferritic steel (A508) and an austenitic steel (316L). The bonding process consists of a combination of heat (980 °C) and pressure (8 MPa) during a constant stage of 35 min. This processing route leads to specific microstructures and mechanical properties which differ from the original ones. In particular the ferrite becomes harder and more brittle due to the thermal cycle of the joining process. Similar results have been found in [3,4] where it was shown that the transition region was shifted from the range −100 to 0 °C to the range 10 to 80 °C after heat treatment.

The ferritic–austenitic joints in the current study were not post-bond heat treated to restore the initial properties in order to keep the interdiffusion zone as small as possible. A batch of ferrite material was also submitted to the same heat treatment as the joints have experienced during the bonding process. This bulk material can be characterized to obtain reference properties of the ferrite. All details of chemical compositions and Microprobe analyses are described in [5].

Mechanical Testing
Mechanical tests were carried out on homogeneous ferritic materials (which have been subjected to the same heat treatment as the joints) and bimaterial joints. Monolithic austenite samples were not available for bulk material property characterization. However, sub-sized specimens were used to obtain some properties (Fig. 1(a)). Several specimen types were used to characterize the materials. This includes: (i) smooth tensile bars, (ii) U-notched tensile bars, (iii) V-notched tensile bars, (iv) sub-size Charpy specimens and single edge notch bend specimens. These specimens are respectively referred to as: TB, NT_χ, ($\chi = 10 \times r/\phi_0$, where r is the notch radius and ϕ_0 the sample diameter at the minimum cross section), NT_V, KCV and SENB. The details of test samples and testing conditions are described in [5].

Table 1. Tensile mechanical properties of both materials

	$R_{p0.2}$ (MPa)	R_m (MPa)	A (%)
A508	568	770	8
316L	264	601	43
Mismatch (A508/316L)	2.15	1.28	0.18
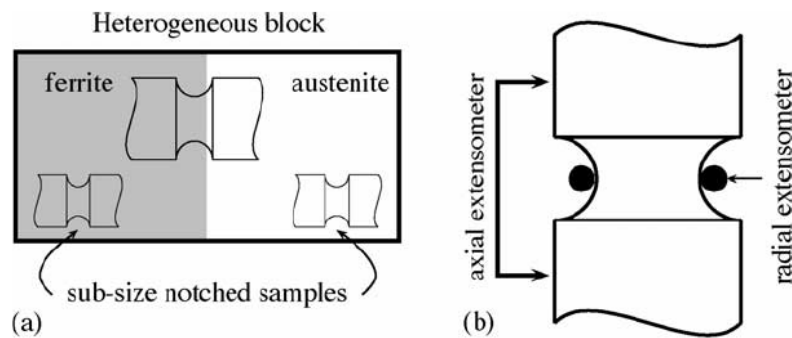
Fig. 1. (a) Notched samples extracted from diffusion bonded heterogeneous blocks. (b) Axial and radial extensometers on NT_χ and NT_V samples.

For tests performed on homogeneous specimen, the sample name is followed by a letter "F" for ferrite or by a letter "A" for austenite in order to identify the material. In the case of heterogeneous specimens, the notch plane is always parallel to the interface. In this case, the letter identifies the material in which the notch lies and a number gives the distance between the notch and the interface. For instance the designation KCV1F represents a Charpy specimen whose notch tip is in the ferrite at a distance of 1mm from the interface.

Fractography Evidence of Crack Path Change
Fractographic examinations of different samples were conducted in order to investigate: (i) the failure mechanisms, (ii) the crack path and crack deflection.

Failure mechanisms are described in [5]. The effect of strength mismatch in heterogeneous specimens on crack paths are illustrated on Fig. 2 in the case of KCV samples. It is shown that in cases where the notch lies in the ferrite, the crack is deviated toward the interface for KCV1F and KCV2F specimens where notch tip distance was 1 and 2 mm, respectively. In the case of the KCV4 ··· 9F specimens the crack runs straight, since the interaction of neighboring materials is not any more effective on the fracture process. For the KCV2F specimen, the interface is crossed by the running crack which further propagates into the austenite. In the case of KCV#A specimens the opposite effect is observed. For KCV1A specimens, the crack tends to propagate away from the interface. The effect is reduced for KCV2A specimens. Otherwise the crack runs straight (KCV4A).Very similar and consistent trends were observed on SENB specimens.
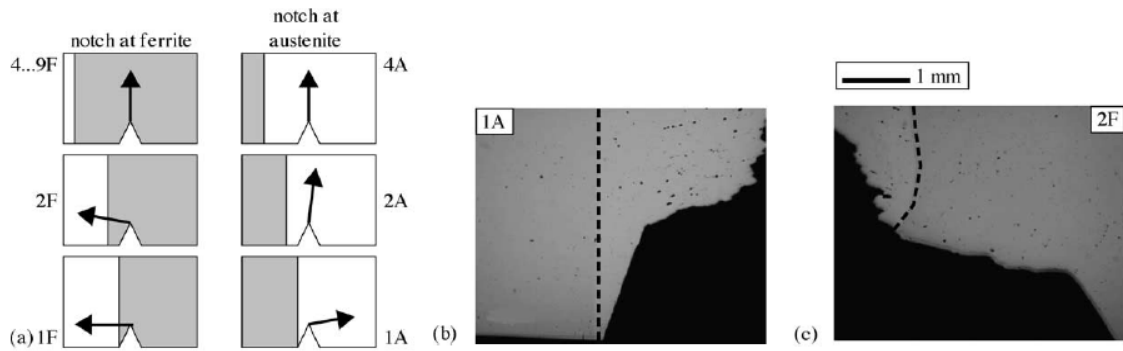
Fig. 2. Crack paths (arrows) observed on Charpy specimens for different locations (A and F) and distances between the notch tip and the interface. Schematic (a) is showing the fracture paths developed with respect to different locations and distances to the bi-material interfaces, (b) notch in austenite at a distance of 1 mm, (c) notch in ferrite at distances of 2 mm. The dashed line delineates the ferrite/austenite interface.
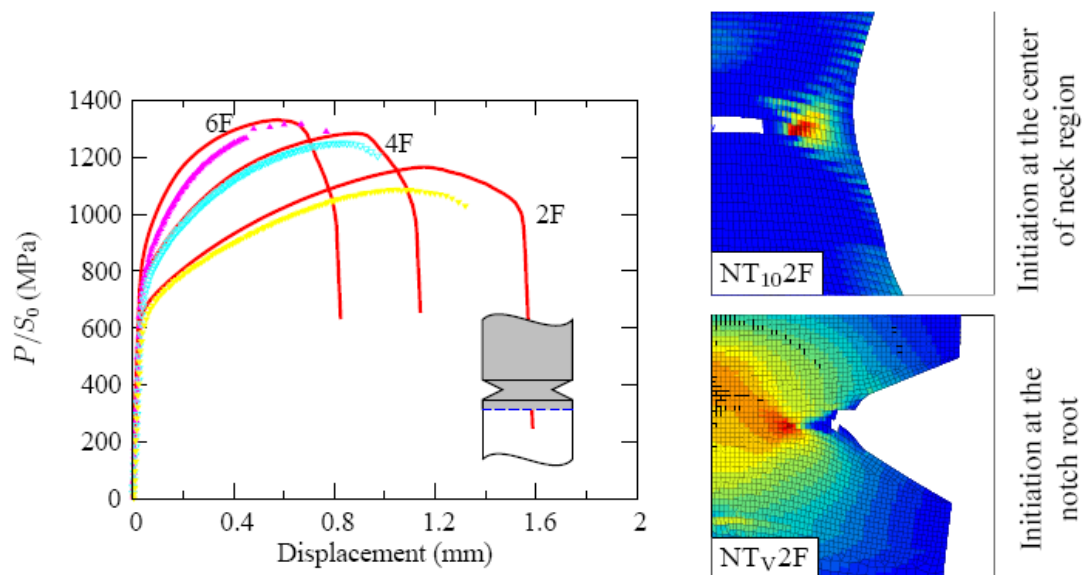
Fig. 3. Testing of axisymmetric bimaterial notched specimens: Results for NT_V specimens. Dashed lines correspond to the FE simulation. Maps show the predicted initiation of the crack.

Results of Mechanical Tests

The complete results of mechanical testing are presented in [5]. The elasto-plastic behavior of the ferritic material can directly be obtained from the tensile tests. The plastic behavior of the austenite was determined using an inverse identification procedure. Standard tensile properties for both materials are given in Table 1. The ferritic steel has a much higher yield strength with a mismatch equal to 2.15, a lower strain to fracture and a lower hardening rate than the austenitic steel.

Ductile fracture was studied using axisymmetric notched tensile bars (Fig. 1(b)). Results obtained from NT_V samples are shown in Fig. 3. Due to the sharp notch, failure is always initiated at the notch root. When the notch is located in the ferrite ($NT_V2F\cdot\cdot\cdot NT_V6F$), decreasing distance to the interface causes the apparent ductility to increase and the maximum load to decrease. The ductility increase is partially caused by the deformation of the austenite along the 13mm gage length. In all cases, stable crack growth initiated at the notch root (which can be observed visually) occurs during the load drop and preceded final failure. Results for Charpy specimens are shown in Fig. 5 for samples with the notch located in the ferrite. In these case, failure initiation corresponds to a ductile mechanism but is followed by brittle failure.

SIMULATION–DISCUSSION

In this section, an interpretation of the main experimental results is proposed based on an application of the local approach to fracture [1]. The method relies on finite element calculations of test pieces which are used to predict crack initiation as well as crack direction of propagation (crack path). Finite element calculations were carried out using axisymmetric, 2D plane strain or 3D elements with linear interpolation and full integration. Finite strain formalism is used.

Materials models
The modelling of damage in both constituents is based on the Gurson model [2]. This model uses a single damage variable which represents the void volume fraction f (also called porosity). The model is based on the definition of a flow potential Φ which depends both on the von Mises stress σ_{eq} and on the pressure σ_m:

$$\Phi = \left(\frac{\sigma_{eq}}{\sigma_0}\right)^2 + 2q_1 f_* \cosh\left(\frac{3}{2}q_2\frac{\sigma_m}{\sigma_0}\right) - 1 - q_1 f_*^2 = 0 \tag{1}$$

σ_0 is the yield stress of the matrix. q_1 and q_2 are constant parameters introduced on a phenomenological basis to better fit damage growth kinetics. f_* is an effective porosity. It is a function of the actual porosity f which has been introduced by Tvergaard and Needleman [6] (GTN model) to represent void coalescence leading to final fracture. It is assumed that coalescence starts at a critical porosity f_c. For actual porosities f larger than f_c, the mechanical softening due to void growth is larger than what is predicted by the original Gurson model [2]. Based on these assumptions, the simplest phenomenological form for f_* is expressed as:

$$f_* = \begin{cases} f & \text{if } f < f_c \\ f_c + \delta(f - f_c) & \text{if } f > f_c \end{cases} \tag{2}$$

where $\delta > 1$ is a coefficient representing the increased damaging effect of porosity. Both f_c and δ have to be adjusted. Failure occurs when $f_* = 1/q_1$. The plastic flow is obtained using the normality rule so that the plastic strain rate tensor is given by:

$$\underline{\dot{\varepsilon}}_{ep} = (1-f)\,\dot{p}\,\frac{\partial \Phi}{\partial \underline{\sigma}} \tag{3}$$

where $\underline{\sigma}$ is the stress tensor and $\dot{p}$ the von Mises equivalent plastic strain rate. Damage evolution is represented by the change in void volume fraction which is obtained applying mass conservation so that:

$$\dot{f} = (1-f)\,trace\,\underline{\dot{\varepsilon}}_{ep} + A_n\,\dot{p}, \tag{4}$$

where the second right hand-side term corresponds to strain controlled nucleation. It is also important to determine or adjust the initial value for the porosity f_0.

Plastic behaviour

The elasto-plastic behavior of the ferritic material can directly be obtained from the tensile tests. The plastic behavior of the austenite was determined using an inverse identification procedure. It was adjusted in order to match the mechanical response of sub–size homogeneous NT_{10} and heterogeneous NT_χ and NT_V samples. This identification strategy for the behavior of different materials is particularly interesting in the case of welds where it is difficult to obtain bulk material representative of the heat affected zone or instance. A similar procedure using notched samples was proposed in [7]. The identified hardening behavior is given y the following equation for the ferritic material (MPa):

$$\sigma_y(p) = 543 + 243(1 - \exp(-49.76p)) + 337(1 - \exp(-2.12p)), \tag{5}$$

and the austenite material by (MPa):

$$\sigma_y(p) = 259 + 1047(1 - \exp(-1.80p)) + 114(1 - \exp(-5.03p)), \tag{6}$$

where p is the equivalent von Mises plastic strain. All materials were assumed to be isotropic.

Ductile damage and failure

In this part, one is interested in cases where the notch lies in the ferrite so that only the damage of ferrite was studied. Damage parameters need to be adjusted on structure undergoing significant damage as well as stable crack growth. For this purpose, both homogeneous NT_χ specimens and heterogeneous NT_V samples were used. To perform the identification of damage parameters (f_0, f_c, δ, A_n, q_1, q_2) experimental results were compared with FE simulations: (i) f_0, f_c and δ were adjusted to represent the sharp load drop on NT_χ samples (corresponding to the initiation of the crack (point A on Fig. 5)),

(ii) A_n was adjusted to obtain the correct crack path on NT_V samples. The softening nature of the constitutive equations leads to strain and damage localization so that FE calculations are mesh size dependent. In this case simulations are carried out using a fixed element size (100 μm in regions where damage develops) and geometry (meshing the whole structure: the symmetries were not used). A good fit was obtained for notched bars using the following parameters (Table 3).
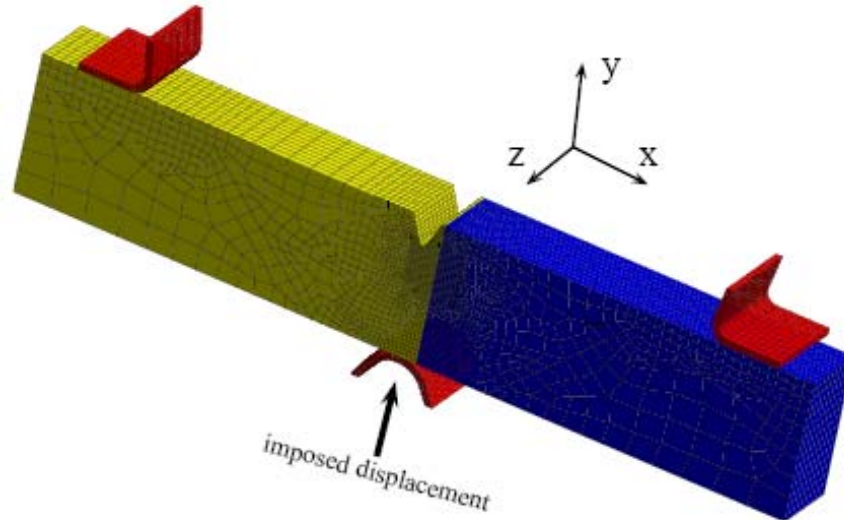
Fig. 4. 3D mesh used for the simulation of heterogeneous KCV1F specimen.

Table 3. Damage parameters of ferrite.

f_0	f_c	δ	q_1	q_2	Mesh size (μm)	A_n		
$2. \, 10^{-4}$	0.1	2.83	1.5	1.25	100	0.04	if	$0.15<p<0.75$

Simulation of Heterogeneous Charpy Specimens
Charpy tests were modeled using 2D plane strain or 3D calculations. The finite element mesh used to model the test is shown on Fig. 4. Contact between the sample, the support and the striker was also modeled assuming a friction coefficient equal to 0.1. The material is considered as broken when f reaches $1/q_1$. The behavior is then replaced by an elastic behavior with a very low stiffness (Young's modulus: E = 1 MPa). Elements where all Gauss points are broken are automatically removed from the calculation.

Results of the simulation are shown in Fig. 5 for case KCV1F where the V-notch lies in the ferrite. In particular, a good agreement is obtained for 3D calculation comparing force—displacement curves. Plane strain calculations overestimate the load and predict an earlier failure. Experimental pop-in for the ferrite is not taken into account as it corresponds to brittle crack extension. Predicted failure initiation is delayed for 3D calculation. Simulated crack paths are shown on Fig. 5 for the KCV1F (3D case) and KCV2F (2D case). Crack defection is reproduced although crack angle is under estimate

in the 3D case whereas a better fit is obtained in the 2D case. It is also shown that the crack grows along the interface once it has reached it. This corresponds to the actual cracking behaviour. Note that, due to the softening behaviour, results are mesh dependant (mesh size, element type, mesh orientation). Use of non-local technique [8] together with a finer mesh could help improving crack prediction.
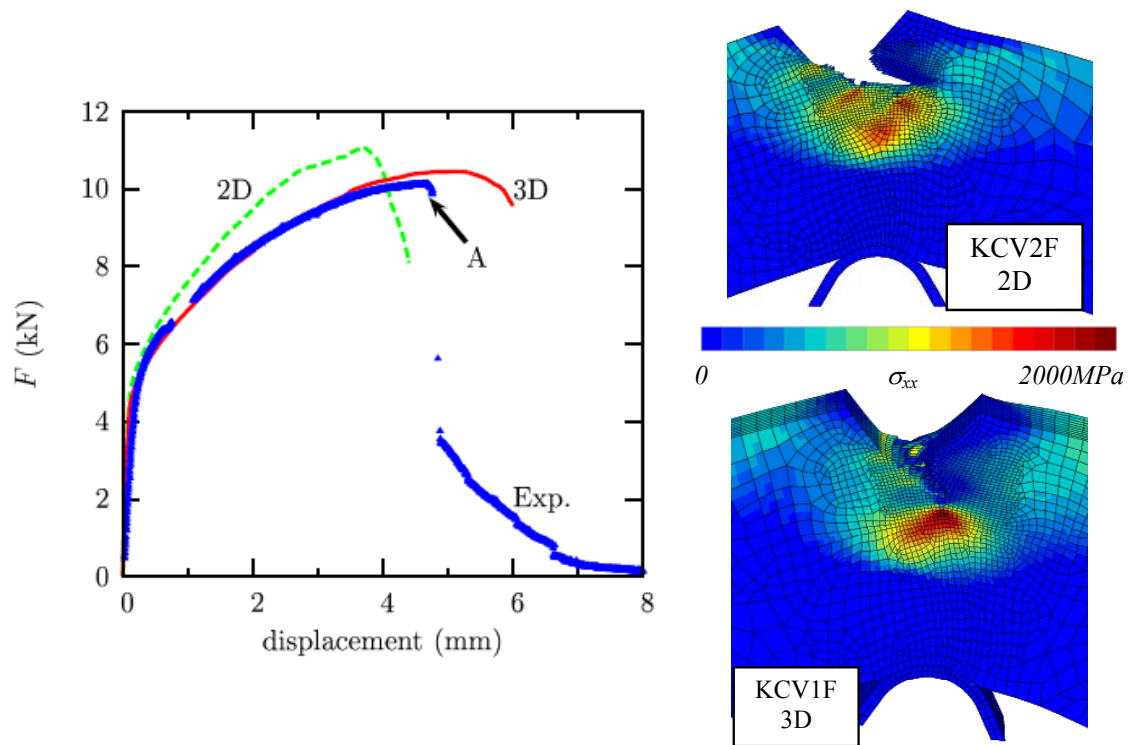
Fig. 5. Charpy tests under static loading: force–deflection curves for samples whose notches are in the ferrite for specimen KCV1F. Dashed and Continuous lines correspond respectively to the 2D and 3D FE simulation. Maps show the predicted crack path.

REFERENCES

1. Pineau, A. (1992). in: Topics in Fracture and Fatigue, pp 197–234, A. Argon (Ed.), Springer Verlag Inc., New York.
2. Gurson, AL. (1977) J. Eng. Mat. Technol. 99, 2–15.
3. Isacsson, M., Narstrom, T. (1998) Mater. Sci. Eng. A 241, 169–178.
4. Narstrom, T., Isacsson, M. (1999) Mater. Sci. Eng. A 271, 224–231.
5. Besson, J., Madi, Y. (2005) Mater. Sci. and Eng. A 397, 84–91.
6. Tvergaard, V., Needleman, A. (1984) Analysis of cup-cone fracture in a round tensile bar. Acta Metall 32, 157–169.
7. Zhang, Z., Hauge, M., Thaulow, C., Ødegsård, J. (2002) Eng. Fract. Mech, 353–366.
8. Mediavilla, J., Peerlings, R.H.J. (2006) Eng. Fract. Mech. 73, 895–916.